Piezoelectric Energy Harvesting and Dissipation on Structural Damping

J. R. LIANG AND W. H. LIAO*

Smart Materials and Structures Laboratory, Department of Mechanical and Automation Engineering
The Chinese University of Hong Kong, Shatin, N. T., Hong Kong, China

ABSTRACT: This article aims to provide a comparative study on the functions of piezoelectric energy harvesting, dissipation, and their effects on the structural damping of vibrating structures. Energy flow in piezoelectric devices is discussed. Detailed modeling of piezoelectric materials and devices are provided to serve as a common base for both analyses of energy harvesting and dissipation. Based on these foundations, two applications of standard energy harvesting (SEH) and resistive shunt damping (RSD) are investigated and compared. Furthermore, in the application of synchronized switch harvesting on inductor (SSHI), it is shown that the two functions of energy harvesting and dissipation are coexistent. Both of them bring out structural damping. Further analyses and optimization for the SSHI technique are performed.

Key Words: energy harvesting, energy dissipation, vibration damping, piezoelectric material, SSHI.

INTRODUCTION

WIRELESS sensor networks (WSNs) can be deployed to monitor the health of military and civil infrastructures (Liao et al., 2001). Different from the traditional sensor systems, these widely distributed networks put more emphasis on the energy issue because of their nature of wireless connections (Raghunathan et al., 2002). Yet, nowadays, most of the devices used in WSNs are still battery-driven. The use of batteries in these devices restricts both their lifespan and installation in places where batteries are hard to replace. This situation would be completely changed if such devices could scavenge energy themselves from their ambient environment. Starting with this motivation, over the past few years the techniques of energy harvesting have been put under the spotlight (Paradiso and Starner, 2005; Beeby et al., 2006; Anton and Sodano, 2007).

One of the promising sources from which people could collect energy is mechanical vibration. Three transduction mechanisms (i.e., piezoelectric, electromagnetic, and electrostatic) were studied in order to reclaim the ambient vibration energy and turn it into useful electrical power. Among generators based on these three mechanisms, the piezoelectric ones are the simplest to fabricate (Beeby et al., 2006); therefore, they are particularly suitable for implementation in microsystems.

Up to now, most of the research on piezoelectric energy harvesting has been mainly concerned with the absolute amount of energy that can be harvested from vibrating structures (Ottman et al., 2002; Badel et al., 2005; Anton and Sodano, 2007). The effect, which results from energy harvesting and reactions to the vibrating structure, was seldom discussed in these studies. Lesieutre et al. (2004) discussed such an issue and claimed that the harvesting of electrical energy from the piezoelectric system brings out structural damping. On the other hand, it has been known for a long time that the effect of structural damping can be caused by energy dissipation. In most of the shunt damping treatments, energy dissipation was regarded as the only function that contributes to structural damping (Moheimani, 2003). The two applications of standard energy harvesting (SEH) and resistive shunt damping (RSD), even though their main functions are energy harvesting and energy dissipation, respectively, can be compared in terms of damping capabilities (Lesieutre et al., 2004).

Referring to the comparison between the two applications, we note that it is possible that the two functions can coexist in a certain condition and both effect structural damping. This phenomenon happens in the application of synchronized switch harvesting on inductor (SSHI). In this article, the relationship among the functions of energy harvesting, dissipation, and their effects on structural damping will be investigated. This understanding is crucial towards developing an adaptive energy harvesting technique. In the section 'Energy Flow in

*Author to whom correspondence should be addressed.
E-mail: whliao@cuhk.edu.hk
Figures 9, 10 and 15 appear in color online: http://jim.sagepub.com

1045-389X/09/05 0515–13 $10.00/0 DOI: 10.1177/1045389X08098194

Piezoelectric Devices', we give an explanation of the two functions of energy harvesting and dissipation in terms of energy flow, in order to clarify some terms for the following discussions. In the section 'Piezoelectric Device Modeling, in terms of Impedance', we propose an impedance-based piezoelectric device model, which can serve as a common base for energy harvesting and dissipation analyses. In the section 'Energy Harvesting and Dissipation', the key concepts and results of SEH and RSD optimizations are reviewed and discussed. Then a comparison between these two applications in terms of damping capabilities is made, concerning coupling coefficients. In the section 'Energy Harvesting and Dissipation of SSHI', after proposing a model that generalizes SEH and SSHI, we discuss the effect on damping contributed by both energy harvesting and dissipation, and further analyze the energy harvesting and damping capabilities for SSHI. Finally, a conclusion is given in the section 'Conclusion'.

ENERGY FLOW IN PIEZOELECTRIC DEVICES

In most of the literature, damping is the dissipation of the energy of a mechanical system (Harris, 1996; de Silva, 2005), and dissipation usually means the lost energy is converted into heat (Wikipedia). However, de Silva (2005) also pointed out that damping is the process that converts and dissipates mechanical energy into other forms of energy. Considering piezoelectric energy harvesting, which also results in structural damping, the previous definitions need to be clarified. In this section, energy flow in piezoelectric devices is studied; afterwards, terms are specified in order to investigate various effects in the following sections.

An Overview of Energy Involved

First, the energy involved in piezoelectric devices will be clarified. Figure 1 shows the single degree-of-freedom (SDOF) schematic representation of piezoelectric devices. Regardless of the purposes of structural damping or energy harvesting, their mechanical parts in the structures are similar. The main differences lie in their shunt circuits. Figure 2 provides an overview of the three forms of energy involved in these devices. These three forms are: mechanical, electrical, and thermal. The first two are linked by the bi-directional piezoelectric transducer. At the same time, either mechanical or electrical energy can be converted into thermal energy by dissipation elements such as mechanical dampers or electrical resistors. Once the energy is dissipated, i.e., transformed into heat, it will not be recovered in the devices, therefore dissipative transformation is uni-directional.

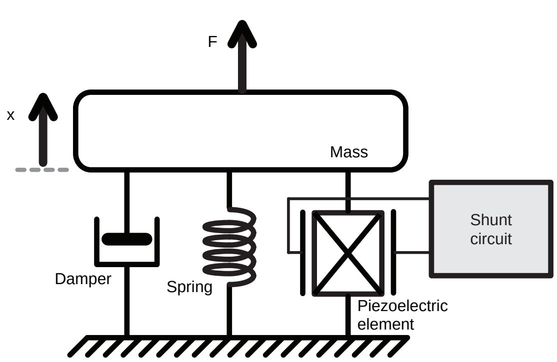

Figure 1. *Schematic representation of piezoelectric devices.*

From the energy flow shown in Figure 2, we can sort out three paths. With path ①, mechanical energy is directly dissipated, thus it represents the function of *mechanical energy dissipation*. Path ② and path ③ both pass through the 'piezoelectric bridge', converting a portion of the mechanical energy into electrical energy. They differ in that some of the electrical energy is converted into heat via path ②, while some of it is converted via path ③ into energy storage. Therefore, path ② is related to energy dissipation in electrical way, or briefly *electrical energy dissipation*; path ③ is related to *electrical energy harvesting*. Mechanical dissipation seems unrelated to piezoelectric transducers, but in fact they have some relation. Since piezoelectric transducers are bi-directional, in some cases, such as active constrained layer damping treatment (Stanway et al., 2003) and active-passive hybrid piezoelectric networks (Tang and Wang, 2001), piezoelectric elements are used to suppress the mechanical vibration so as to enhance mechanical energy dissipation.

Term Specification

The three paths in Figure 2 represent three *functions* that can remove energy from the vibrating structure with

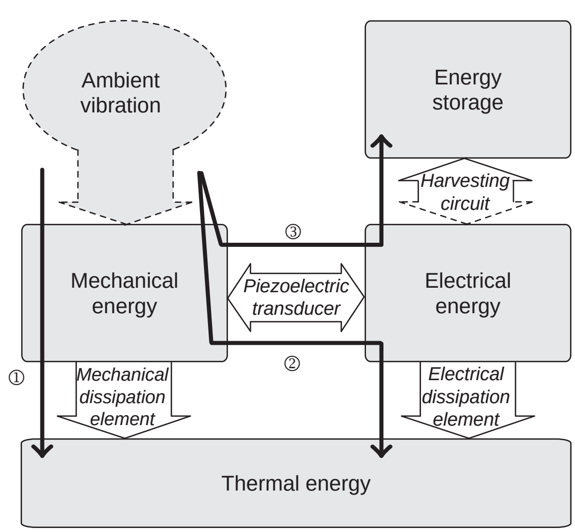

Figure 2. *Energy flow chart of piezoelectric devices.*

the piezoelectric transducer. One or more of these functions can take place in certain applications and cause the *effect* of structural damping. Table 1 gives the term specification for four functions that can remove mechanical energy from vibrating structures. To have a complete classification, this table includes the item ④, *mechanical energy harvesting*. For example, in automatic watches, with an elaborately designed mechanism, mechanical energy can be stored in the mainsprings to drive the watches. This technique has been successfully applied for more than 80 years.

With the above specification, when considering the damping applications, e.g., RSD, we emphasize the total effect of the involved functions on the structure. On the other hand, when considering the applications of energy harvesting, e.g., SEH or SSHI, we focus on the utilization of the electrical energy harvesting function. However, this does not mean that there is no other function in the system. On the contrary, in the applications of energy harvesting, parasitic mechanical and electrical energy dissipations usually exist. In general, these were not considered in the previous research. But since they partake and dissipate some of the energy that could be harvested, these functions would become important for the purpose of harvesting energy from vibration sources where exploitable energy is limited.

The three factors within the parentheses in Table 1 are indices to evaluate the corresponding functions or effect. For traditional damping, the term *loss factor* was usually used to evaluate the total damping capability. It was defined as the ratio between the energy dissipated per cycle and the energy associated with vibration (Warkentin and Hagood, 1997). Here, in order to continue using this term for damping evaluation, we make a subtle change in this old definition. The new defined loss factor is the ratio between the energy removed per cycle and the energy associated with vibration. Moreover, considering energy harvesting, it is not enough to show the detailed energy relations with the use of loss factor only. Therefore, two additional factors are defined with respect to energy harvesting and energy dissipation, as follows.

Table 1. Term specification.

Path	Function		Effect
①	Mechanical energy dissipation	Energy dissipation (dissipation factor, η_d)	Vibration damping (loss factor, η_Σ)
②	Electrical energy dissipation		
③	Electrical energy harvesting	Energy harvesting (harvesting factor, η_h)	
④	Mechanical energy harvesting		

For energy harvesting, the new term *harvesting factor* is defined to evaluate the harvesting capability as:

$$\eta_h = \frac{E_h}{2\pi E_{\max}} \tag{1}$$

where E_h denotes the harvested energy in one cycle, $E_{\max}$ is the energy associated with vibration.

For energy dissipation, the term *dissipation factor* is used to evaluate the dissipation capability as:

$$\eta_d = \frac{E_d}{2\pi E_{\max}} \tag{2}$$

where E_d is the dissipated energy in one cycle.

With Equations (1) and (2), we can define the *loss factor* as:

$$\eta_\Sigma = \frac{\Delta E}{2\pi E_{\max}} = \eta_h + \eta_d \tag{3}$$

where ΔE is the summation of E_h and E_d, which represents the total removed energy from the vibrating structure in one cycle.

PIEZOELECTRIC DEVICE MODELING, IN TERMS OF IMPEDANCE

To compare the damping effect between energy harvesting and energy dissipation, we should first have a common representation of piezoelectric elements. As given in IEEE Standard on Piezoelectricity (1987), the linear piezoelectricity can be represented by four sets of constitutive equations, as follows:

$$\begin{bmatrix} T_p \\ D_i \end{bmatrix} = \begin{bmatrix} c^E_{pq} & -e_{kp} \\ e_{iq} & \varepsilon^S_{ik} \end{bmatrix} \begin{bmatrix} S_q \\ E_k \end{bmatrix} \tag{4}$$

$$\begin{bmatrix} S_p \\ D_i \end{bmatrix} = \begin{bmatrix} s^E_{pq} & d_{kp} \\ d_{iq} & \varepsilon^T_{ik} \end{bmatrix} \begin{bmatrix} T_q \\ E_k \end{bmatrix} \tag{5}$$

$$\begin{bmatrix} S_p \\ E_i \end{bmatrix} = \begin{bmatrix} s^D_{pq} & g_{kp} \\ -g_{iq} & \beta^T_{ik} \end{bmatrix} \begin{bmatrix} T_q \\ D_k \end{bmatrix} \tag{6}$$

$$\begin{bmatrix} T_p \\ E_i \end{bmatrix} = \begin{bmatrix} c^D_{pq} & -h_{kp} \\ -h_{iq} & \beta^S_{ik} \end{bmatrix} \begin{bmatrix} S_q \\ D_k \end{bmatrix} \tag{7}$$

where T, S, D, and E denote the stress, strain, electric displacement, and electric field, respectively; d, e, g, and h are piezoelectric constants; c is elastic stiffness constant; s is elastic compliance constant; ε is permittivity constant; β is impermittivity constant; the subscripts are tensor notations; the superscripts T, S, D, and E denote the corresponding parameters at constant stress, strain, electric displacement, and electric field, respectively. Either one of these four can be used to describe the same coupling characteristics of piezoelectric materials. In the studies of traditional damping, Equation (5) was usually used (Hagood and von Flotow, 1991; Clark, 2000; Moheimani, 2003); while in the studies of energy harvesting, Equation (4) was more popular (Badel et al., 2005; Shu et al., 2007); but still, there were exceptions (Lesieutre and Davis, 1997; Ng and Liao, 2005; Roundy, 2005).

This section begins with the dynamic representations of these four sets of constitutive equations, in terms of impedance. Based on these, we select one as the common basis of our analysis and then obtain the device model and equivalent circuit.

Dynamic Representations

Suppose a piezoelectric element, whose dimensions are shown in Figure 3, is bonded on a vibrating beam, and is working under 3–1 mode. Assuming the motion wavelength is much larger than l; and l, w are much larger than the thickness t, four dimensional relations can be obtained:

$$F = twT_1, \quad x = l\,S_1, \quad U = -tE_3, \quad Q = wlD_3 \tag{8}$$

where F, x denote the force and displacement in the '1' direction; U, Q denote the voltage across and charge stored in the '3' direction. Substituting Equation (8) into Equation (4) yields the macroscopic piezoelectric equations:

$$\begin{bmatrix} F \\ Q \end{bmatrix} = \begin{bmatrix} \dfrac{tw}{l} c_{11}^{E} & we_{31} \\ we_{31} & -\dfrac{wl}{t}\varepsilon_{33}^{S} \end{bmatrix} \begin{bmatrix} x \\ U \end{bmatrix}. \tag{9}$$

Equation (9) does not explicitly show the dynamic behavior of the piezoelectric patch. To study the dynamic behavior, two derivative relations between electrical current and charge, mechanical velocity, and displacement are needed, i.e.:

$$I = -Qs, \qquad v = xs \tag{10}$$

where I denotes current, v denotes velocity, and s is the Laplace operator. Substituting Equation (10) into Equation (9) yields:

$$\begin{bmatrix} F \\ I \end{bmatrix} = \begin{bmatrix} K^E/s & \alpha_e \\ -\alpha_e & sC^S \end{bmatrix} \begin{bmatrix} v \\ U \end{bmatrix} \tag{11}$$

where:

$$K^E = \frac{tw}{l} c_{11}^{E}, \quad C^S = \frac{wl}{t}\varepsilon_{33}^{S}, \quad \alpha_e = we_{31} \tag{12}$$

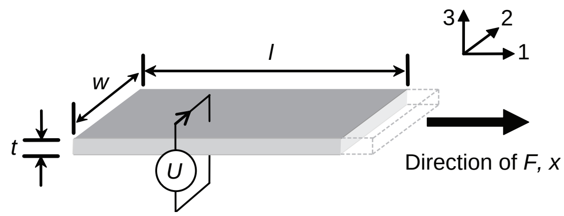

Figure 3. *Schematic diagram of piezoelectric patch.*

are the short circuit stiffness, clamped capacitance, and force–voltage coupling factor of the piezoelectric patch, respectively.

For illustration, Figure 4(a) shows the schematic diagram corresponding to Equation (11). Note that K^E/s represents the mechanical impedance of the short circuit stiffness in '1' direction, and $1/(sC^S)$ represents the electrical impedance of the clamped capacitance in '3' direction. This model regards the mechanical part as the patch's stiffness in parallel with a force source, and the electrical part as the capacitance in parallel with a current source. We call this P–P model in brief, where 'P' stands for parallel relation. Similarly, for the other three constitutive equations, i.e., Equations (5)–(7), we can derive the P–S, S–S, S–P models corresponding to Figure 4(b)–(d), where 'S' stands for series relation, and α_g is velocity–current coupling factor.

Since those four dynamic models illustrated in Figure 4 are compatible with the analyses of mechanical impedance networks and electrical ones, they can provide us with a guideline for selection of constitutive equations in the analyses of piezoelectric devices. For instance, from the electrical point of view, it would be more convenient to use P–P or S–P models to analyze devices whose shunt circuit network is built up by parallel connecting impedances; P–S or S–S models are preferred for shunt networks built up in series.

Device Model

Based on Equation (5), Hagood and von Flotow (1991) also drew a macroscopic representation for the electrical part of the piezoelectric materials, and included shunt impedance in the governing equations. This process altered the equations to 'half device level', thus making it possible to consider the piezoelectric patch and its shunt circuit as a whole. Also, consider the dynamic definition of device coupling coefficient given by:

$$k_d^2 = \frac{(\omega^D)^2 - (\omega^E)^2}{(\omega^D)^2} \tag{13}$$

where ω^D is the open circuit natural frequency, ω^E is the short circuit natural frequency. Compared to the

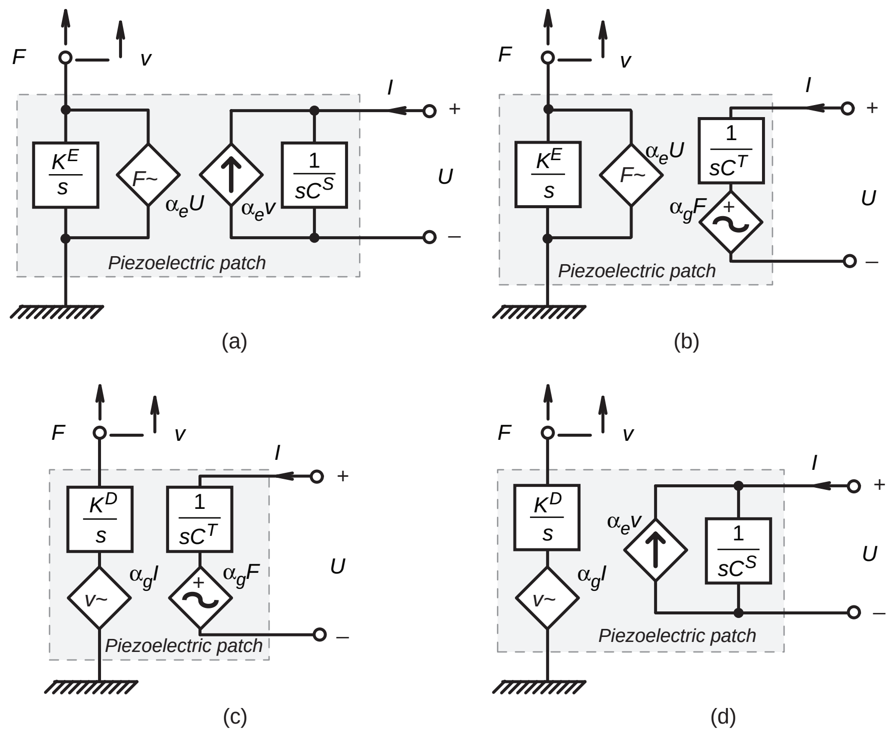

Figure 4. *Schematic diagrams corresponding to four sets of constitutive equations. (a) P–P model. (b) P–S model. (c) S–S model. (d) S–P model.*

electromechanical coupling coefficient of the piezoelectric element (Badel et al., 2005):

$$k_e^2 = \frac{\alpha_e^2}{K^E C^S + \alpha_e^2} \tag{14}$$

this dynamic definition is again in 'half device level', since the measurements of ω^D and ω^E regard the mechanical part of the device as a whole, but exclude the shunt circuit from the device.

Referring to these two analyses at either electrical or mechanical device level, and based on our representations for piezoelectric materials, we form an integrative device model by extending the P–P model of piezoelectric materials. The mounting piezoelectric patch on the beam structure can be modeled with mechanical impedances in parallel (Badel et al., 2005), and electrical shunt circuit appears in parallel to the inherent piezoelectric capacitance (Hagood and von Flotow, 1991). As illustrated in Figure 5, the device model is given as:

$$\begin{bmatrix} F \\ I \end{bmatrix} = \begin{bmatrix} \sum Z_{\text{mech}}^E & \alpha_e \\ -\alpha_e & \sum Y_{\text{elec}}^S \end{bmatrix} \begin{bmatrix} v \\ U \end{bmatrix} \tag{15}$$

where:

$$\sum Z_{\text{mech}}^E = \frac{K^E}{s} + Z_{\text{mech}} \tag{16}$$

$$\sum Y_{\text{elec}}^S = sC^S + Y_{\text{elec}} \tag{17}$$

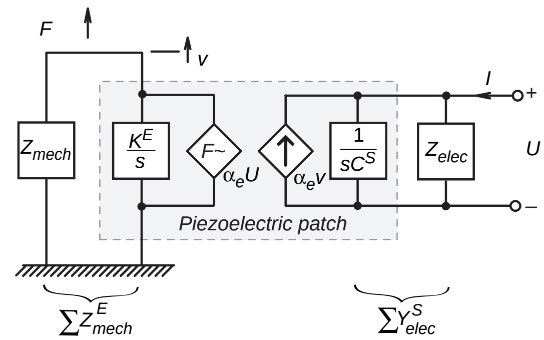

Figure 5. *Piezoelectric device model.*

and Z_{mech} is the total external mechanical impedance; $Y_{\text{elec}} = Z_{\text{elec}}^{-1}$, is the total external electrical admittance.

In particular, if the electrical part is purely composed of impedances, i.e., the current I in Equation (15) and Figure 5 equals to zero, simplifying Equation (15) with this condition yields the expression of the *equivalent mechanical impedance*:

$$Z_{\text{mech-eq}} = F/v = \sum Z_{\text{mech}}^E + \alpha_e^2 \, Z_{\Sigma\text{elec}}^S \tag{18}$$

where $Z_{\Sigma\text{elec}}^S = \left(\sum Y_{\text{elec}}^S\right)^{-1}$ is the total electrical impedance.

Equivalent Circuit

With the equivalent mechanical impedance given in Equation (18), the piezoelectric device can be regarded as a pure mechanical device. On the other hand, in order to study the electrical behavior of the device, we can also make the device equivalent to a pure electrical circuit. To keep voltages across and currents through all electrical elements unchanged, the equivalent circuit can be characterized in form of the Ohm's Law as:

$$\frac{u_{\text{eq}}}{i_{\text{eq}}} = \frac{\sum Z^E_{\text{mech}}}{\alpha_e^2} + Z^S_{\Sigma\text{elec}} \tag{19}$$

where u_{eq} and i_{eq} are equivalent voltage and current associated with mechanical force and velocity. Their relationships were given by Warkentin and Hagood (1997) as:

$$\begin{cases} u_{\text{eq}} & = F/\alpha_e \\ i_{\text{eq}} & = v\alpha_e \end{cases}. \tag{20}$$

In most of the previous analyses and also our study presented in this article, the external mechanical structure is regarded as a part of the vibration source, which excites the piezoelectric patch. Therefore, the mechanical part only includes the patch's short circuit stiffness. With this, Equation (19) can be specified as:

$$\frac{u_{\text{eq}}}{i_{\text{eq}}} = \frac{1}{sC_{\text{eq}}} + \frac{1}{sC^S + Y_{\text{elec}}} \tag{21}$$

where C_{eq} is the equivalent capacitance corresponding to the short circuit stiffness of the piezoelectric patch, with the following relation:

$$C_{\text{eq}} = \frac{\alpha_e^2}{K^E}. \tag{22}$$

According to Equation (21), the equivalent circuit diagram is shown in Figure 6(a). In the figure, S_{eq} is the equivalent voltage source representing the sinusoidal force excitation applied to the patch structure. This equivalent circuit can serve as a common base for damping analyses with both energy harvesting and energy dissipation. It depends on whether a shunt circuit designed for energy harvesting or energy dissipation is connected.

Moreover, the circuit can be further simplified with an additional approximation that the coupling coefficient $k_e^2 \to 0$. From Equation (14), such approximation results in $C_{\text{eq}} \ll C^S$. Therefore, $1/(sC_{\text{eq}})$, as electrical impedance, is dominant. In this case, S_{eq} and C_{eq} together form a current source S'_{eq}. The simplified equivalent circuit is shown in Figure 6(b).

In traditional passive damping, the simplified equivalent circuit shown in Figure 6(b) was seldom used, since the approximation $k_e^2 \to 0$ contradicts the purpose of extracting as much mechanical energy as possible. Hagood and von Flotow (1991) proposed an inspired analysis for shunt damping optimization,

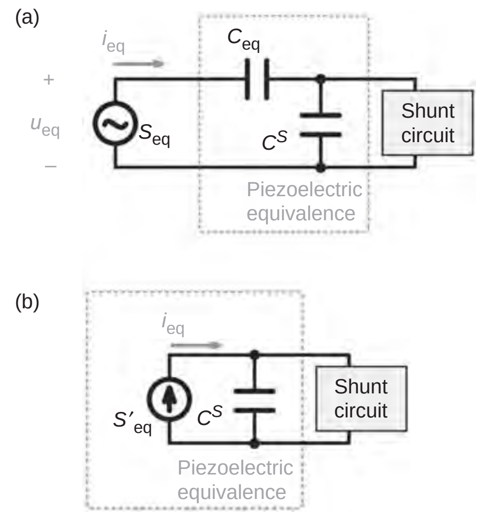

Figure 6. *Equivalent circuit diagrams of a piezoelectric device. (a) Equivalent circuit. (b) Simplified equivalent circuit.*

which can also be derived from the equivalent circuit in Figure 6(a). Later work in this area mainly focused on multiple mode vibration damping methods (Moheimani, 2003).

In the research of energy harvesting, up to now, most of the analyses were based on the simplified equivalent circuit as shown in Figure 6(b) (Ottman et al., 2002; Lesieutre et al., 2004; Guyomar et al., 2005; Badel et al., 2005; Makihara et al., 2006; Anton and Sodano, 2007). As a result, the counteraction of the shunt circuit to the mechanical structure was usually neglected. In fact, more universal analysis based on SEH circuit and the piezoelectric equivalent circuit as shown in Figure 6(a) was once proposed with the title 'nonlinear shunt damping' (Warkentin and Hagood, 1997), before the recent research on energy harvesting.

The concept of loss factor is important for evaluating damping performance. But in energy harvesting, since most of the studies were based on the simplified equivalent circuit, only the absolute harvested energy can be know. Up to now, different piezoelectric generators were usually compared with their absolute harvesting power (Beeby et al., 2006). In order to provide a better understanding, we suggest that the *relative energy harvesting capability* should also be considered. Based on the equivalent circuit shown in Figure 6(a), in the following analysis we discuss the relative energy harvesting performance with the new term 'harvesting factor', which was defined in the previous section.

ENERGY HARVESTING AND DISSIPATION

Besides the majority of literature studying absolute energy or power that can be harvested from an ideal current source, Lesieutre et al. (2004) have discussed the structural damping effect due to energy harvesting in the application of SEH. In terms of damping capability, which is evaluated by the loss factor, this effect can be compared to RSD. The comparison made by Lesieutre et al. (2004) was only valid under the condition that $k_e^2 \to 0$. In this section, a brief review of the optimizations of SEH and RSD will be given; afterwards, general comparisons covering the whole range of k_e^2 will be made.

Standard Energy Harvesting

In the SEH application, only the energy harvesting function contributes to the effect of structural damping. The shunt circuit is a nonlinear circuit, which is composed of a bridge rectifier, a filter capacitor, and other loads in parallel. Its equivalent circuit is shown in Figure 7. In analyzing this circuit, the DC filter capacitor C_{rect} is assumed to be large enough so that the voltage across this capacitor V_{rect} is nearly constant (Ottman et al., 2002). For the 'nonlinear damping' circuit proposed by Warkentin and Hagood (1997), it differs from the circuit in Figure 7 in that the C_{rect} is replaced by a constant DC voltage supply. Yet, their analyses are compatible.

The ratio between the harvested energy and energy associated with vibration in one cycle, which is called *harvesting factor* in this article, is a function of k_e^2 and $\tilde{V}_{\text{rect}}$ (Warkentin and Hagood, 1997):

$$\eta_h = \frac{4}{\pi}\tilde{V}_{\text{rect}}\frac{1-\tilde{V}_{\text{rect}}}{\frac{1-k_e^2}{k_e^2}+\tilde{V}_{\text{rect}}} \tag{23}$$

where $\tilde{V}_{\text{rect}}$ is obtained by non-dimensionalizing the rectified voltage to the amplitude of open circuit voltage, i.e.:

$$\tilde{V}_{\text{rect}} = \frac{V_{\text{rect}}}{V_{oc}} \tag{24}$$

The coupling coefficient of the piezoelectric element depends on material and geometry properties, which cannot be changed after the device is made. The maximum harvesting factor can be obtained as follows:

$$\eta_{h,\max} = \frac{4}{\pi}\frac{\left(1-\sqrt{1-k_e^2}\right)^2}{k_e^2} \tag{25}$$

at a non-dimensional rectified voltage:

$$\tilde{V}_{\text{rect,opt}} = \frac{1-k_e^2}{k_e^2}\left(\sqrt{\frac{1}{1-k_e^2}}-1\right). \tag{26}$$

The optimum rectified voltage can be achieved by properly choosing the load. This load can be an adaptive

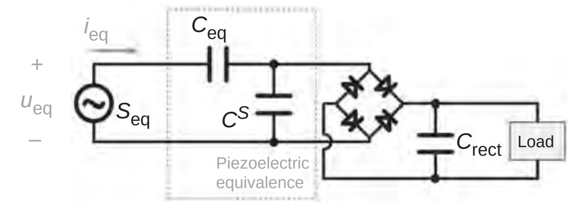

Figure 7. *Equivalent circuit for SEH.*

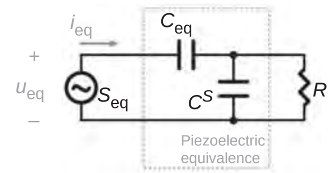

Figure 8. *Equivalent circuit for RSD.*

DC–DC converter (Ottman et al., 2002) or optimal resistor (Guyomar et al., 2005). The extracted power is transferred or consumed so as to keep the optimum rectified voltage constant. In addition, it can be proven that when $k_e^2 \to 0$, $\tilde{V}_{\text{rect,opt}} = 0.5$, which is the optimal result given by Ottman et al. (2002). In their study on the damping effect of SEH, Lesieutre et al. (2004) took $\tilde{V}_{\text{rect,opt}}$ as constant, i.e., equal to 0.5, regardless of k_e^2, therefore, their optimum non-dimensional rectified voltage and maximum harvesting factor[1] are only valid when $k_e^2 \to 0$.

Resistive Shunt Damping

In the application of RSD (Hagood and von Flotow, 1991), only the energy dissipation function contributes to the effect of structural damping. The equivalent circuit is shown in Figure 8. It only connects a resistor as its shunt circuit to dissipate the extracted energy, thus resulting in damping. The dissipation factor is given by:

$$\eta_d = \frac{\rho\, k_e^2}{1-k_e^2+\rho^2} \tag{27}$$

where ρ is the non-dimensional frequency:

$$\rho = RC^S\omega \tag{28}$$

and ω is the excitation angular frequency, R is the resistance of the shunt resistor. The maximum dissipation factor can be obtained as follows:

$$\eta_{d,\max} = \frac{k_e^2}{2\sqrt{1-k_e^2}} \tag{29}$$

at a non-dimensional frequency of:

$$\rho_{\text{opt}} = \sqrt{1-k_e^2}. \tag{30}$$

[1]Loss factor was used in their study. In this paper, harvesting factor is used instead, while loss factor was defined in the section 'Energy Flow in Piezoelectric Devices'.

Comparison between SEH and RSD

To compare the characteristics between SEH and RSD, we employ the non-dimensional voltage–charge diagrams to illustrate their energy conversion cycles.

Since the equivalent current in Figure 6(a) equals $v\alpha_e$, the equivalent charge input is the integral of this current, which is $x\alpha_e$, where x is the displacement of the mechanical source, i.e., the integral of the velocity v. Assuming X as the maximum displacement, the maximum equivalent input charge should be $X\alpha_e$. Non-dimensionalizing $x\alpha_e$ with $X\alpha_e$, we have:

$$\tilde{q}_{\text{eq}} = \frac{x\alpha_e}{X\alpha_e} = \frac{x}{X} = \tilde{x}. \tag{31}$$

It is not only the non-dimensional equivalent input charge $\tilde{q}_{\text{eq}}$, but also the non-dimensional displacement $\tilde{x}$ induced by the mechanical source. Similarly, we can also non-dimensionalize the equivalent input voltage F/α_e with respect to the maximum voltage across C_{eq}:

$$\tilde{u}_{\text{eq}} = \frac{F/\alpha_e}{X\alpha_e/C_{\text{eq}}} = \frac{F}{K^E X} = \tilde{F}. \tag{32}$$

The non-dimensional equivalent input voltage $\tilde{u}_{\text{eq}}$ is also the non-dimensional force $\tilde{F}$ applied to the piezoelectric patch.

Given the situation that $k_e^2 = 0.3$, for instance, the energy conversion cycles for SEH with optimum $\tilde{V}_{\text{rect}}$ and RSD with optimum ρ are shown in Figures 9 and 10, respectively. The black solid curve in each diagram shows the relation between non-dimensional charge and non-dimensional voltage in one cycle. The areas of blue and green ellipses represent 2π multiplying the maximum stored energy in the devices: blue for electrical and green for mechanical.[2] The areas enclosed by the $\tilde{q} - \tilde{u}$ loci represent the energy removed from the structures in one cycle. But in order to distinguish whether the extracted energy is harvested or dissipated, different patterns are used in the diagrams.

The main differences between Figures 9 and 10 are the shapes of the $\tilde{q} - \tilde{u}$ loci and the patterns that fill the areas enclosed by the loci. But even though the flows of the extracted energy in these two applications are different, they can be compared in terms of damping capability, which is evaluated by the loss factor. Without energy being dissipated, the harvesting factor in SEH is also the loss factor; similarly, without energy being harvested, the dissipation factor in RSD is also the loss factor.

According to the relations given in Equations (25) and (29), the two maximum loss factors, i.e., $(\eta_{\Sigma,\max})_{\text{SEH}}$ and $(\eta_{\Sigma,\max})_{\text{RSD}}$, in the two applications, as functions of k_e^2, are compared in Figure 11. As k_e^2 increases, the attainable maximum loss factors for both applications

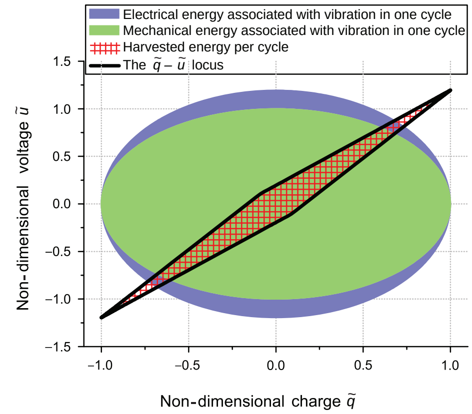

Figure 9. Energy cycle for SEH.

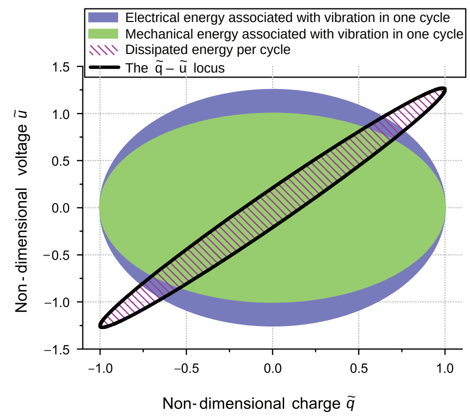

Figure 10. Energy cycle for RSD.

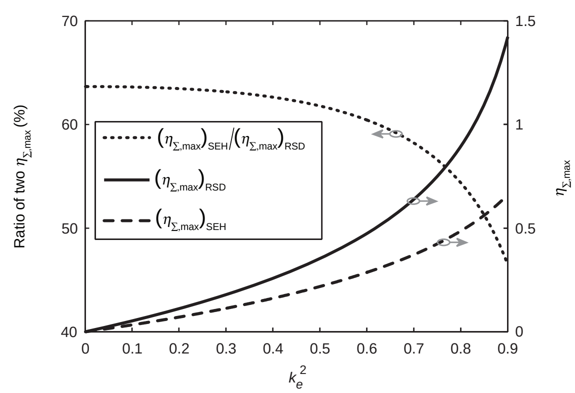

Figure 11. Maximum loss factors in the two applications and their ratio.

increase; also, the ratio between the two factors of SEH and RSD decreases. Moreover, it should be noted that, when coupling coefficient of the piezoelectric element approaches zero, we can obtain:

$$\lim_{k_e^2 \to 0} \frac{(\eta_{\Sigma,\max})_{\text{SEH}}}{(\eta_{\Sigma,\max})_{\text{RSD}}} = \frac{2}{\pi} = 63.66\% \tag{33}$$

which can also be observed from the dot curve in Figure 11. Lesieutre et al. (2004) found the same result

[2]Diagrams in color appear in online version. For grayscale printing, the electrical and mechanical energy is represented by darker and lighter gray patches, respectively.

under this special condition. Indeed most of the previous analyses on SEH took $k_e^2 \rightarrow 0$ as their premise, explicitly or implicitly. This premise constrains the endeavor to increase the material coupling in order to harvest more energy. It simplifies the analysis; however, it confines the optimization to specific, rather than general, conditions.

ENERGY HARVESTING AND DISSIPATION OF SSHI

In the previous two applications, each has only one dominant function that contributes to the effect of structural damping. In the application of SSHI, the situation is more complicated. Both of the two functions, energy harvesting and energy dissipation, coexist in this application, and bring out damping effect. Previous research on SSHI was conducted for the only purpose of harvesting energy; nevertheless, unlike the application of SEH, considering its contribution to structural damping, the function of energy harvesting may not be dominant in all situations. Detailed study of the relationship between energy harvesting, dissipation and their effects on SSHI can help us better understand the energy flow and conversion mechanism within the piezoelectric devices.

The SSHI Technique

The technique of SEH provides a passive solution to harvest ambient vibration energy. It is simple and reliable; however, its harvesting capability is difficult to further enhance. As the electrical part of the device is composed of C^S in parallel with the shunt circuit, Figure 12 shows the typical waveforms of the voltage across it, the current ($\alpha_e v$) flowing into it, and its power input (product of voltage and current). In most of the cycle the power is positive, which means that energy is converted from mechanical into electrical; but in some intervals it has negative value, which indicates that the energy returns from electrical part to mechanical part. We call this *energy return phenomenon*.

In order to enhance the energy conversion efficiency, Guyomar et al. (2005) proposed a solution called *SSHI* (Badel et al., 2005; Shu et al., 2007). The equivalent circuit and typical voltage, current, and power waveforms of this technique are shown in Figures 13 and 14, respectively. This technique was further specified as ‘parallel-SSHI’ by Lefeuvre et al. (2006). By involving the shunt path composed of an active switch *sw* and a small inductor L, with appropriate control of the switch, this circuit can overcome the energy return phenomenon so as to make sure the power always flows into the electrical part.

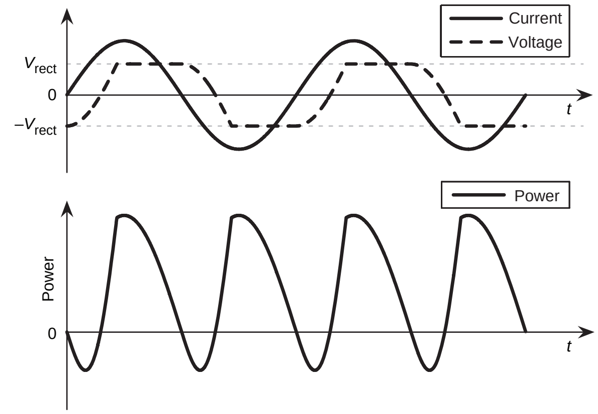

Figure 12. *Typical voltage, current and power waveforms in SEH.*

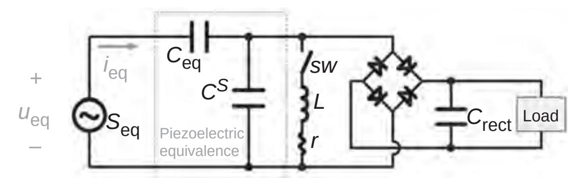

Figure 13. *Equivalent circuit for energy harvesting with SSHI technique.*

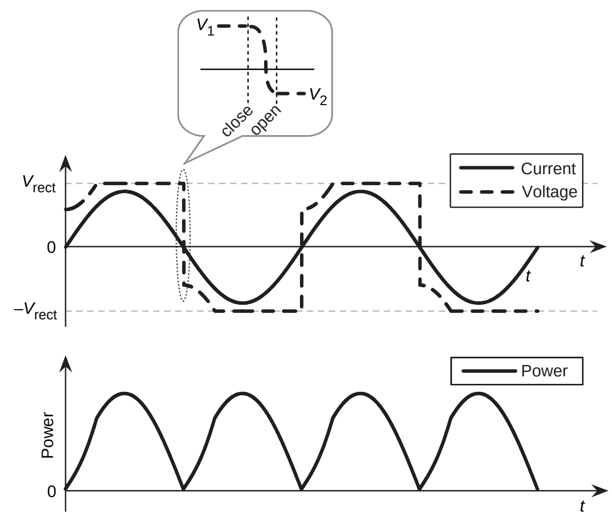

Figure 14. *Typical voltage, current and power waveforms in energy harvesting with SSHI technique.*

The switch is off in most of the cycle; it takes action at the time when the current equals to zero. Also at this instant, the charge stored in C^S is at its extreme value. During the operation, the switch is first turned on to create a ‘shortcut’ for the charge stored in C^S, and then turned off to disconnect the shortcut again when the voltage across C^S alters to another extreme value. The electrical cycle, which is decided by the time constant LC^S, is much shorter than the mechanical cycle. The response time can be neglected, so the voltage waveform can be regarded as changing from V_1 to V_2 steeply at the instant when the current equals to zero. The zoom-in view of the action instant is also shown in Figure 14.

General Representation for Shunt Energy Harvesting

Most references on SSHI gave the relation between V_2 and V_1 in terms of electrical quality factor Q. In order to make a more general representation, we take:

$$\frac{V_2}{V_1} = \gamma, \quad -1 < \gamma \leqslant 0 \text{ or } \gamma = 1. \tag{34}$$

When $\gamma = 1$, it represents the SEH. When γ is negative, it can represent energy harvesting with SSHI technique under any electrical Q value, since in this situation:

$$\gamma = -e^{-\frac{\pi}{2Q}}. \tag{35}$$

For a practical inductor, there is always parasitic resistance, which is denoted as r in Figure 13. If no additional energy is provided to the C^S and 'shortcut' loop, γ can never reach -1.

Coexistent Energy Harvesting and Dissipation in SSHI

Most of the research on harvesting with SSHI technique focused on the optimization in order to harvest more energy from the mechanical source (Guyomar et al., 2005; Badel et al., 2005; Lefeuvre et al., 2006; Shu and Lien, 2006; Shu et al., 2007), while the electrical energy dissipation was considered in the simulation by Badel et al. (2005). The energy dissipation corresponds to the voltage change from V_1 to V_2 across C^S. Till now, no further analytical result is given, especially of the relationship between energy harvesting and energy dissipation in this application.

As mentioned above, the functions of energy harvesting and energy dissipation coexist in this application. The amount of energy harvested in one cycle is:

$$E_h = 2C^S V_{\text{rect}}[2V_{oc} - V_{\text{rect}}(1+\gamma)] \tag{36}$$

while the amount of energy dissipated in one cycle is:

$$E_d = C^S V_{\text{rect}}^2 (1 - \gamma^2). \tag{37}$$

Besides, when $\gamma \leqslant 0$, no energy returns from the electrical part to the source. The energy associated with vibration only includes the strain energy, which is:

$$E_{\max} = \frac{aC^S V_{oc}^2}{2} \tag{38}$$

where a stands for the ratio of:

$$a = \frac{1 - k_e^2}{k_e^2}. \tag{39}$$

The relations among E_h, E_d and $2\pi E_{\max}$ can be illustrated in the non-dimensional voltage–charge diagram.

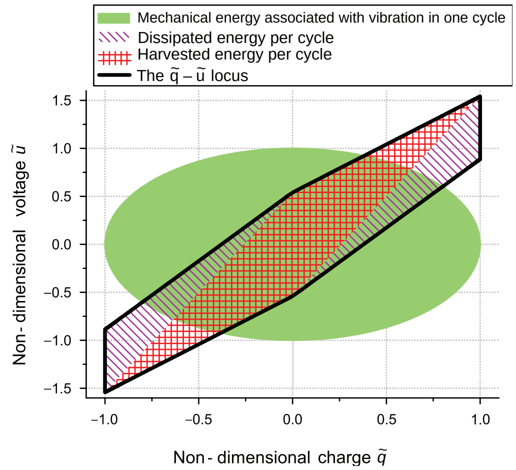

Figure 15. *Energy cycle for energy harvesting with SSHI technique.*

For example, given the situation where $k_e^2 = 0.3$, $\gamma = -0.2$, i.e., $Q \approx 1.0$, the energy conversion cycle for harvesting energy with SSHI technique under optimum situation is shown in Figure 15. The steep voltage changes at maximum charge enable the $\tilde{q} - \tilde{u}$ locus to enclose more area. Compared with the SEH and RSD, whose energy conversion cycles are shown in Figures 9 and 10, energy harvesting with SSHI technique is capable to extract more energy in one cycle. Within a cycle, some of the extracted energy is converted into heat, i.e., dissipated, while the rest is harvested and kept in some suitable electrical energy storage devices (Sodano et al., 2005a,b; Guan and Liao, 2007, 2008).

Substituting Equations (36)–(38) for E_d, E_h, and $E_{\max}$ into Equations (1) and (2), the harvesting factor and dissipation factor of this device can be obtained as:

$$\eta_h = \frac{4\tilde{V}_{\text{rect}} - 2\tilde{V}_{\text{rect}}^2(1+\gamma)}{a\pi} \tag{40}$$

$$\eta_d = \frac{\tilde{V}_{\text{rect}}^2(1-\gamma^2)}{a\pi} \tag{41}$$

where $\tilde{V}_{\text{rect}}$ is given by Equation (24). According to Equation (3), the loss factor η_Σ is the sum of η_h and η_d:

$$\eta_\Sigma = \frac{4\tilde{V}_{\text{rect}} - \tilde{V}_{\text{rect}}^2(1+\gamma)^2}{a\pi}. \tag{42}$$

In addition, since the harvesting factor η_h given in Equation (40) and the loss factor η_Σ given in Equation (42) should not be negative, there is a practical range of $\tilde{V}_{\text{rect}}$, which is:

$$0 \leqslant \tilde{V}_{\text{rect}} \leqslant \frac{2}{1+\gamma}. \tag{43}$$

In this interval, when k_e^2 and γ are fixed, η_d and η_Σ monotonously increase with $\tilde{V}_{\text{rect}}$, yet η_h is a

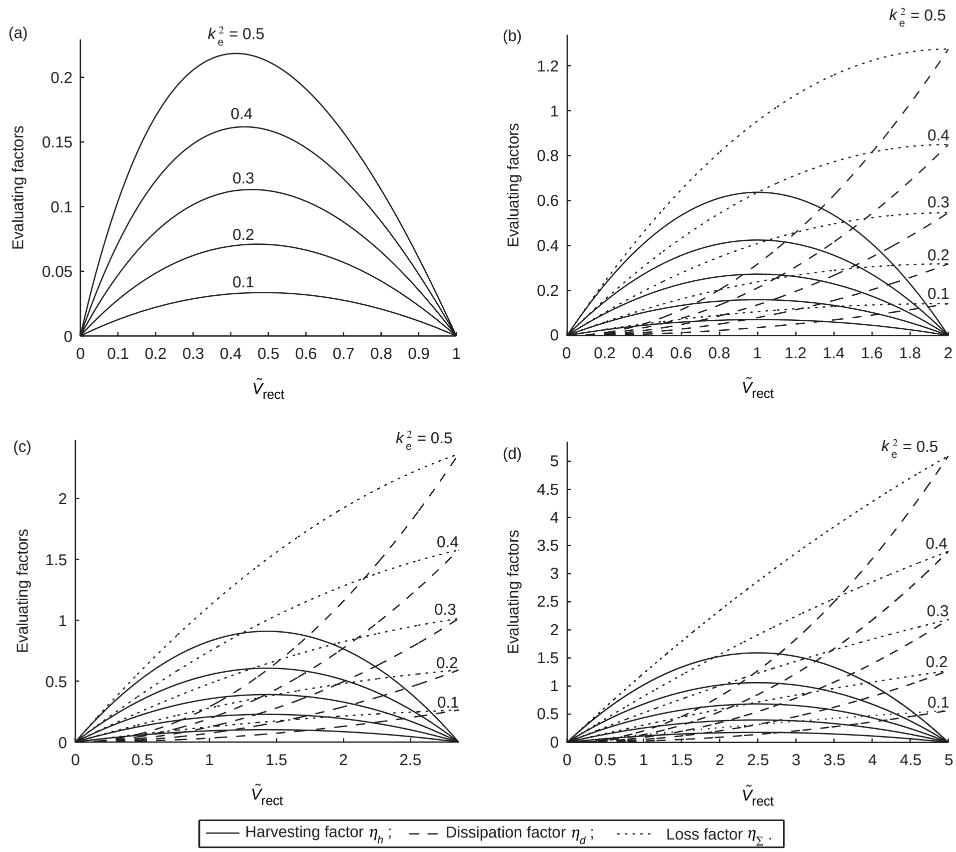

Figure 16. *Evaluating factors, as functions of $\tilde{V}_{rect}$ and k_e^2, under different values of γ. (a) $\gamma = 1$ (SEH); (b) $\gamma = 0$ ($Q = 0$); (c) $\gamma = -0.3$ ($Q = 1.3$); (d) $\gamma = -0.6$ ($Q = 3.1$).*

non-monotonic function. The maximum value of η_h can be obtained:

$$\eta_{h,\max} = \frac{2}{a\pi(1+\gamma)} \tag{44}$$

at an optimum non-dimensional rectified voltage:

$$\tilde{V}_{\text{rect, opt}} = \frac{1}{1+\gamma}. \tag{45}$$

It should be noted that the optimum rectified voltages for maximum harvesting factor are one half of its applicable range, as given in Equation (43).

According to Equations (40)–(43), the harvesting factor, dissipation factor and loss factor, as functions of $\tilde{V}_{rect}$ and k_e^2, are evaluated with four different values of γ. The results of these three evaluating factors are shown in Figure 16. Figure 16(a) stands for the situation of SEH.[3] Ideally, no energy is dissipated in this situation, thus the dissipation factor equals zero; the curves of harvesting factor overlap with those of loss factor. As γ decreases, under the same k_e^2 and $\tilde{V}_{rect}$, all the three factors increase. In addition, it can also be seen from Figure 16 that when $\tilde{V}_{rect}$ reaches its upper limit, there is no energy harvesting effect, i.e., $\eta_h = 0$, thus all structural damping effect is due to energy dissipation. In this special case, this device becomes a *synchronized switch damping on inductor* (SSDI) device (Guyomar and Badel, 2006). This damping treatment can achieve a large loss factor, which is comparable to those of some high polymers, e.g., for hard rubber and polystyrene, whose loss factors are 1.0 and 2.0, respectively (Cremer et al., 2005).

With the intention to optimize SSHI, considering the proportional relations between harvesting factor and dissipation factor shown in Figure 16, two guidelines are suggested. First, for SSHI with the same k_e^2 and γ, there are two $\tilde{V}_{rect}$ corresponding to the same harvesting factor η_h; yet the smaller one should be the preference. Its corresponding dissipation factor is smaller, therefore, less energy is dissipated within one cycle with the same harvesting performance. The saved energy can be harvested in the future cycles. Second, for SSHI under $\tilde{V}_{\text{rect, opt}}$, even though $\eta_{h,\max}$ increases against γ, the smaller γ is not necessary the better. Since η_d at $\tilde{V}_{\text{rect, opt}}$ also increases against γ, its increasing rate is even larger than that of $\eta_{h,\max}$. In other words, the ratio between the dissipated energy and harvested energy increases with γ. Therefore, rather than merely enhancing the harvesting capability, a more optimized SSHI should also take

[3]Equations (23)–(26) are used for this sub-figure.

these into account in order to make a good balance between the coexistent energy harvesting and energy dissipation.

Energy Harvesting and Damping Performances of SSHI

Besides clarifying the relation of energy harvesting, dissipation, and damping in SSHI, we can also theoretically prove the advantages of the SSHI technique. In terms of energy harvesting capability, we can non-dimensionalize the maximum harvesting factors of SSHI to those of SEH under the same coupling coefficients, as:

$$\tilde{\eta}_{h,\max} = \frac{(\eta_{h,\max})_{\mathrm{SSHI}}}{(\eta_{h,\max})_{\mathrm{SEH}}}. \quad (46)$$

Figure 17(a) shows the non-dimensional maximum harvesting factor $\tilde{\eta}_{h,\max}$ as function of k_e^2 under different values of γ. It shows that, for the purpose of harvesting energy, the harvesting capability of SSHI technique is better than that of SEH, regardless of k_e^2 and γ, since all $\tilde{\eta}_{h,\max}$ in Figure 17(a) is larger than 1, i.e., 10^0. Moreover, more significant improvements can be achieved by introducing the SSHI treatment to the harvesting devices with higher coupling coefficient, i.e., larger k_e^2. On the other hand, with the same device using SSHI, the smaller γ, the larger improvement can be obtained.

Similarly, in terms of damping capability, we can non-dimensionalize the maximum loss factor of SSHI, which is specified as SSDI, to that of RSD under the same coupling coefficients, as:

$$\tilde{\eta}_{\Sigma,\max} = \frac{(\eta_{\Sigma,\max})_{\mathrm{SSDI}}}{(\eta_{\Sigma,\max})_{\mathrm{RSD}}}. \quad (47)$$

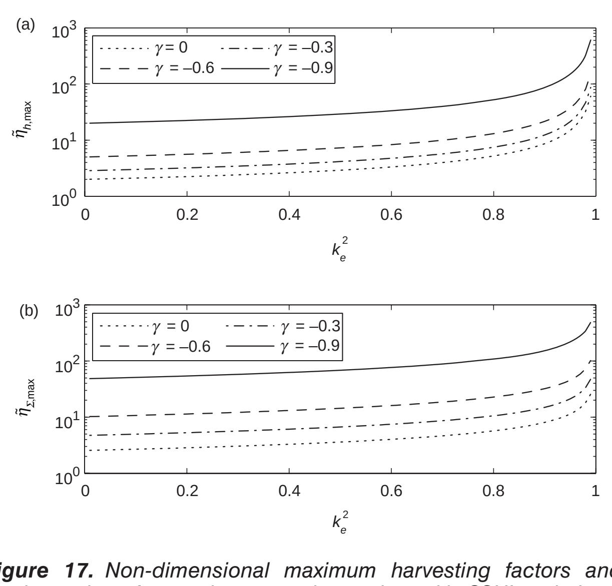

Figure 17. *Non-dimensional maximum harvesting factors and maximum loss factors in energy harvesting with SSHI technique. (a) Harvesting factor. (b) Loss factor.*

Figure 17(b) shows the non-dimensional maximum loss factor $\tilde{\eta}_{\Sigma,\max}$ as function of k_e^2 with respect to different values of γ. The damping capability of SSDI is better than that of RSD. The curves of $\tilde{\eta}_{\Sigma,\max}$ show a similar trend to $\tilde{\eta}_{h,\max}$ in Figure 17(a).

CONCLUSION

In this article, we proposed analyses to clarify the relationship among the functions of energy harvesting, energy dissipation, and their effects on structural damping in piezoelectric devices. Related concepts were discussed and detailed models of piezoelectric devices were provided. Two applications of SEH and RSD utilizing piezoelectric materials were investigated, and the similarities and differences between energy harvesting and energy dissipation were discussed. These two functions could be selected to achieve different objectives. Furthermore, coexistent energy harvesting and dissipation in the implementation of energy harvesting with SSHI technique were investigated. These coexisting functions can both contribute to the effect of structural damping. The performances of the SSHI technique were also investigated. It has been shown that the SSHI would outperform the SEH in terms of harvesting capability and outperform the RSD in terms of damping capability. The results and discussion given in this article will help us develop a more efficient and adaptive piezoelectric energy harvesting system as a promising power source.

ACKNOWLEDGMENTS

The work described in this article was supported by grants from Innovation and Technology Commission (Project No. ITP/011/07AP) and Research Grants Council (Project No. CUHK4152/08E) of Hong Kong Special Administrative Region, China.

REFERENCES

Anton, S.R. and Sodano, H.A. 2007. "A Review of Power Harvesting using Piezoelectric Materials (2003–2006)," *Smart Materials and Structures*, 16(3):R1–R21.

Badel, A., Guyomar, D., Lefeuvre, E. and Richard, C. 2005. "Efficiency Enhancement of a Piezoelectric Energy Harvesting Device in Pulsed Operation by Synchronous Charge Inversion," *Journal of Intelligent Material Systems and Structures*, 16(10):889–901.

Beeby, S., Tudor, M. and White, N. 2006. "Energy Harvesting Vibration Sources for Microsystems Applications," *Measurement Science and Technology*, 17(12):R175–R195.

Clark, W.W. 2000. "Vibration Control with State-switched Piezoelectric Materials," *Journal of Intelligent Material Systems and Structures*, 11(4):263–271.

Cremer, L., Heckl, M. and Petersson, B.A.T. 2005. *Structure-borne Sound: Structural Vibrations and Sound Radiation at Audio Frequencies*, Springer-Verlag, Berlin, Heidelberg.

de Silva, C.W. 2005. *Vibration and Shock Handbook*, CRC Press, Boca Raton, FL, USA.

Guan, M.J. and Liao, W.H. 2007. "On the Efficiencies of Piezoelectric Energy Harvesting Circuits towards Storage Device Voltages," *Smart Materials and Structures*, 16:498–505.

Guan, M.J. and Liao, W.H. 2008. "Characteristics of Energy Storage Devices in Piezoelectric Energy Harvesting Systems," *Journal of Intelligent Material Systems and Structures*, 19(6):671–680.

Guyomar, D. and Badel, A. 2006. "Nonlinear Semi-passive Multimodal Vibration Damping: An Efficient Probabilistic Approach," *Journal of Sound and Vibration*, 294(1–2):249–268.

Guyomar, D., Badel, A., Lefeuvre, E. and Richard, C. 2005. "Toward Energy Harvesting using Active Materials and Conversion Improvement by Nonlinear Processing," *IEEE Transactions on Ultrasonics, Ferroelectrics and Frequency Control*, 52(4):584–595.

Hagood, N.W. and von Flotow, A. 1991. "Damping of Structural Vibrations with Piezoelectric Materials and Passive Electrical Networks," *Journal of Sound and Vibration*, 146:243–268.

Harris, C.M. 1996. *Shock and Vibration Handbook*, McGraw-Hill, New York.

IEEE Standard on Piezoelectricity 1987. *ANSI/IEEE Std 176-1987*.

Lefeuvre, E., Badel, A., Richard, C., Petit, L. and Guyomar, D. 2006. "A Comparison between Several Vibration-powered Piezoelectric Generators for Standalone Systems," *Sensors and Actuators A: Physical*, 126(2):405–416.

Lesieutre, G.A. and Davis, C.L. 1997. "Can a Coupling Coefficient of a Piezoelectric Device be Higher than those of its Active Material?" *Journal of Intelligent Material Systems and Structures*, 8(10):859–867.

Lesieutre, G.A., Ottman, G.K. and Hofmann, H.F. 2004. "Damping as a Result of Piezoelectric Energy Harvesting," *Journal of Sound Vibration*, 269:991–1001.

Liao, W.H., Wang, D.H. and Huang, S.L. 2001. "Wireless Monitoring of Cable Tension of Cable-stayed Bridges using PVDF Piezoelectric Films," *Journal of Intelligent Material Systems and Structures*, 12(5):331–339.

Makihara, K., Onoda, J. and Miyakawa, T. 2006. "Low Energy Dissipation Electric Circuit for Energy Harvesting," *Smart Materials and Structures*, 15(5):1493–1498.

Moheimani, S. 2003. "A Survey of Recent Innovations in Vibration Damping and Control using Shunted Piezoelectric Transducers," *IEEE Transactions on Control Systems Technology*, 11(4):482–494.

Ng, T.H. and Liao, W.H. 2005. "Sensitivity Analysis and Energy Harvesting for a Self-powered Piezoelectric Sensor," *Journal of Intelligent Material Systems and Structures*, 16(10):785–797.

Ottman, G., Hofmann, H., Bhatt, A. and Lesieutre, G. 2002. "Adaptive Piezoelectric Energy Harvesting Circuit for Wireless Remote Power Supply," *IEEE Transactions on Power Electronics*, 17(5):669–676.

Paradiso, J.A. and Starner, T. 2005. "Energy Scavenging for Mobile and Wireless Electronics," *IEEE Pervasive Computing*, 4(1):18–27.

Raghunathan, V., Schurgers, C., Park, S. and Srivastava, M. 2002. "Energy-aware Wireless Microsensor Networks," *IEEE Signal Processing Magazine*, 19(2):40–50.

Roundy, S. 2005. "On the Effectiveness of Vibration-based Energy Harvesting," *Journal of Intelligent Material Systems and Structures*, 16(10):809–823.

Shu, Y.C. and Lien, I.C. 2006. "Analysis of Power Output for Piezoelectric Energy Harvesting Systems," *Smart Materials and Structures*, 15(6):1499–1512.

Shu, Y.C., Lien, I.C. and Wu, W.J. 2007. "An Improved Analysis of the SSHI Interface in Piezoelectric Energy Harvesting," *Smart Materials and Structures*, 16:2253–2264.

Sodano, H.A., Inman, D.J. and Park, G. 2005a. "Generation and Storage of Electricity from Power Harvesting Devices," *Journal of Intelligent Material Systems and Structures*, 16(1):67–75.

Sodano, H.A., Inman, D.J. and Park, G. 2005b. "Comparison of Piezoelectric Energy Harvesting Devices for Recharging Batteries," *Journal of Intelligent Material Systems and Structures*, 16(10):799–807.

Stanway, R., Rongong, J. and Sims, N. 2003. "Active Constrained-layer Damping: A State-of-the-art Review," *Proceedings of the Institution of Mechanical Engineers, Part I: Journal of Systems and Control Engineering*, 217(6):437–456.

Tang, J. and Wang, K.W. 2001. "Active-passive Hybrid Piezoelectric Networks for Vibration Control: Comparisons and Improvement," *Smart Materials and Structures*, 10(4):794–806.

Warkentin, D.J. and Hagood, N.W. 1997. "Nonlinear Piezoelectric Shunting for Structural Damping," In: *Proceedings of SPIE Conference on Smart Structures and Materials*, San Diego, CA, USA, 3041:747–757.

Wikipedia, URL: http://en.wikipedia.org/wiki/Dissipation